

# Geophysical Research Letters

## RESEARCH LETTER

10.1029/2019GL083826

### Key Points:

- Interferometric phases from multiple satellite radar platforms are combined to derive the first comprehensive phase map of Antarctic ice velocity
- The precision in ice speed (20 cm/year) and flow direction (5°) over 80% of Antarctica is a factor 10 better than prior mappings based on feature and speckle tracking
- The product will improve mass balance studies, reconstruction of ice thickness, regional atmospheric climate modeling, and numerical ice sheet modeling

### Supporting Information:

- Supporting Information S1

### Correspondence to:

J. Mouginot,  
 jmouginot@uci.edu

### Citation:

Mouginot, J., Rignot, E., & Scheuchl, B. (2019). Continent-wide, interferometric SAR phase, mapping of Antarctic ice velocity. *Geophysical Research Letters*, 46, 9710–9718. <https://doi.org/10.1029/2019GL083826>




Received 28 MAY 2019

Accepted 10 JUL 2019

Accepted article online 29 JUL 2019

Published online 23 AUG 2019

## Continent-Wide, Interferometric SAR Phase, Mapping of Antarctic Ice Velocity

J. Mouginot<sup>1,2</sup> , E. Rignot<sup>1,3,4</sup> , and B. Scheuchl<sup>1</sup> 

<sup>1</sup>Department of Earth System Science, University of California, Irvine, CA, USA, <sup>2</sup>Université Grenoble Alpes, CNRS, IRD, Grenoble INP, IGE, Grenoble, France, <sup>3</sup>Jet Propulsion Laboratory, California Institute of Technology, Pasadena, CA, USA, <sup>4</sup>Department of Civil and Environmental Engineering, University of California, Irvine, CA, USA

**Abstract** Surface ice velocity is a fundamental characteristic of glaciers and ice sheets that quantifies the transport of ice. Changes in ice dynamics have a major impact on ice sheet mass balance and its contribution to sea level rise. Prior comprehensive mappings employed speckle and feature tracking techniques, optimized for fast-flow areas, with precision of 2–5 m/year, hence limiting our ability to describe ice flow in the slow interior. We present a vector map of ice velocity using the interferometric phase from multiple satellite synthetic aperture radars resulting in 10 times higher precision in speed (20 cm/year) and direction (5°) over 80% of Antarctica. Precision mapping over areas of slow motion (<1 m/year) improves from 20 to 93%, which helps better constrain drainage boundaries, improve mass balance assessment, evaluate regional atmospheric climate models, reconstruct ice thickness, and inform ice sheet numerical models.

**Plain Language Summary** We present a new map of Antarctic ice velocity that is 10 times more precise than prior maps and reveals ice motion at a high precision over 80% of the continent versus 20% in the past. The ice motion vector map provides novel constraints on interior ice motion and its connection with the glaciers and ice stream that control the stability and mass balance of the Antarctic Ice Sheet.

## 1. Introduction

Ice velocity is a fundamental characteristic of glaciers and ice sheets that measures the direction and rate at which ice is transported from the accumulation to the ablation regions (Cuffey & Paterson, 2010). Surface ice motion is measured from space by sequential images of satellite optical and synthetic aperture radar (SAR) data using feature and speckle tracking techniques, respectively (Joughin et al., 2010, 2018; Michel & Rignot, 1999; Mouginot et al., 2017; Mouginot et al., 2012; Nagler et al., 2015; Rignot et al., 2011; Rignot & Mouginot, 2012; Figure 1). The precision of tracking methods depends on the time separation between data acquisition, the spatial resolution of the data, and the signal to noise ratio of the correlation algorithm. Typical precision reaches 2–5 m/year after data stacking in the Antarctic (Mouginot et al., 2017; Figure 2). This level of precision is suitable for calculating ice volume fluxes of fast moving glaciers along the periphery of the ice sheets, where ice speed ranges from hundreds to thousands of meters per year (Mouginot et al., 2019; Rignot et al., 2019), but it is not sufficient to constrain physical processes in the interior regions, such as flow changes, and changes in strain rate or force balance. Indeed, about 60% of Antarctica is flowing at a speed slower than 10 m/year (Rignot et al., 2011). With present-day rates of Antarctic mass loss equivalent to 10–15% of the balance flux (which is the mass flux that keeps the ice sheet in mass equilibrium with the accumulation of snowfall; Rignot et al., 2019), it is of interest to develop a capability to quantify mass fluxes better than 1–2% or 20–40 Gt/year (Gt = 1 billion ton), which translates into a precision in speed along the periphery of 4 to 40 m/year, which we have already achieved, but a precision of the order of 10–20 cm/year in the interior regions, which was not reached in prior mappings. In terms of flow direction, which is important to resolve the pathways of ice from the interior to the margin, this uncertainty in speed translates into an uncertainty in direction of 0.01 radian or 0.6° (Mouginot et al., 2017).

In contrast with speckle and feature tracking, the precision of the interferometric phase is not limited by the spatial resolution of the data (a few meters) but by the size of the radar imaging wavelength (a few centimeters), the time separation between multiple passes (a few days to weeks), and the phase

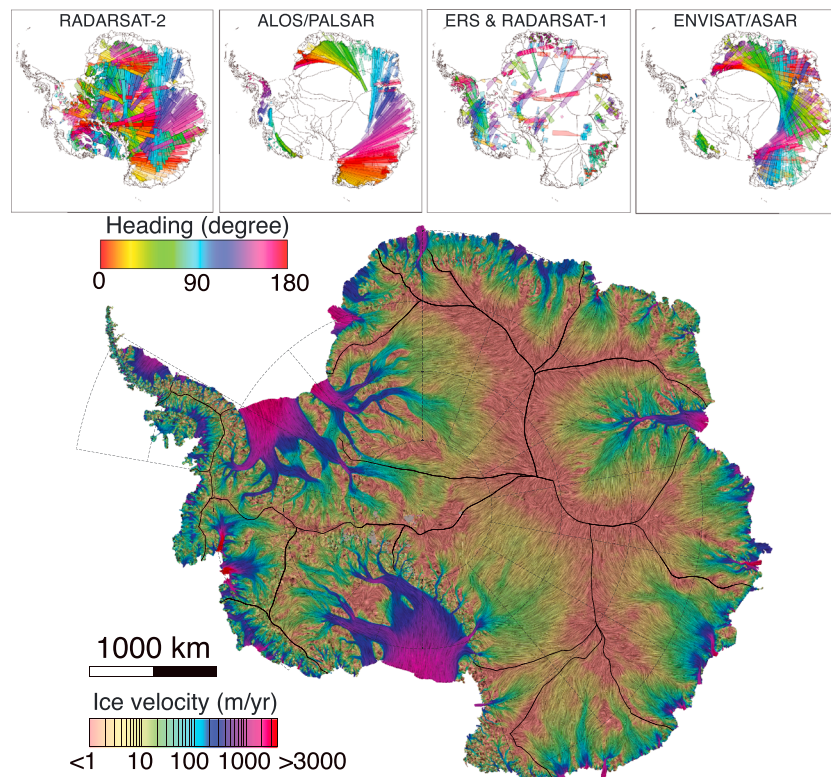


**Figure 1.** Mapping of ice motion in Antarctica using synthetic-aperture radar interferometric phase data. Upper panels show the distribution of data tracks used from the Canadian RADARSAT-2, Japanese ALOS PALSAR, European ERS and Canadian RADARSAT-1, and European Envisat ASAR. Lower main panel shows a complete map of ice motion in Antarctica combining phase data in the interior and speckle tracking in the fast-moving sectors, with speed colored on a logarithmic scale from brown (less than 1 m/year) to red (more than 3 km/year) and flow direction indicated by colored lines and showing the flow pattern of ice across the continent.

signal-to-noise ratio (Richard M. Goldstein et al., 1993; Massonnet et al., 1993). In practice, the interferometric phase measures the ice deformation signal with a precision 1 to 2 orders of magnitude better than speckle tracking, that is, at the millimeter level, which translates into a precision of 10–20 cm/year level with a repeat cycle of several weeks (Table S1 in the supporting information). A drawback of the interferometric phase, however, is that it only measures the line-of-sight motion, that is, deformation in a single look direction, versus both along and across tracks with a single interferometric pair for speckle tracking. When using the interferometric phase, multiple passes at different look angles are therefore required to form a velocity vector, for example, ascending and descending tracks or left and right looking angle tracks (Joughin, 2002; Joughin et al., 1998). To measure ice flow in three dimensions, at least three independent look directions are required (Gray, 2011). A traditional approach for ice sheets has been to assume that ice flows parallel to the ice sheet surface, in which case the ice flow vector is determined from two nearly orthogonal look directions. The surface-parallel flow assumption is reasonable as long as the vertical velocity of the ice is large compared to the surface mass balance component, that is, the rate of change in mass at the ice sheet surface from snowfall, melt, wind transport, and other processes. Surface mass balance values in Antarctica typically range from 10 to 30 cm/year (van Wessem et al., 2018); hence, the surface-parallel flow assumption is reasonable where ice speed is typically greater than 50 cm/yr, which is more than 96% of Antarctica in area (Figure 1).

Historically, there has not been enough quality data or crossing tracks to make vector phase mapping possible in Antarctica. One exception was the Amundsen Sea Embayment (ASE) sector of West Antarctica where a vector phase map was assembled using 1-day repeat Earth Remote Sensing (ERS) 1/2 interferometric data (Rignot et al., 2004). In East Antarctica, too few ascending tracks were acquired by ERS-1/2 to permit vector phase mapping of ice velocity. Over the last 10 years, however, an increase in data acquisition from multiple

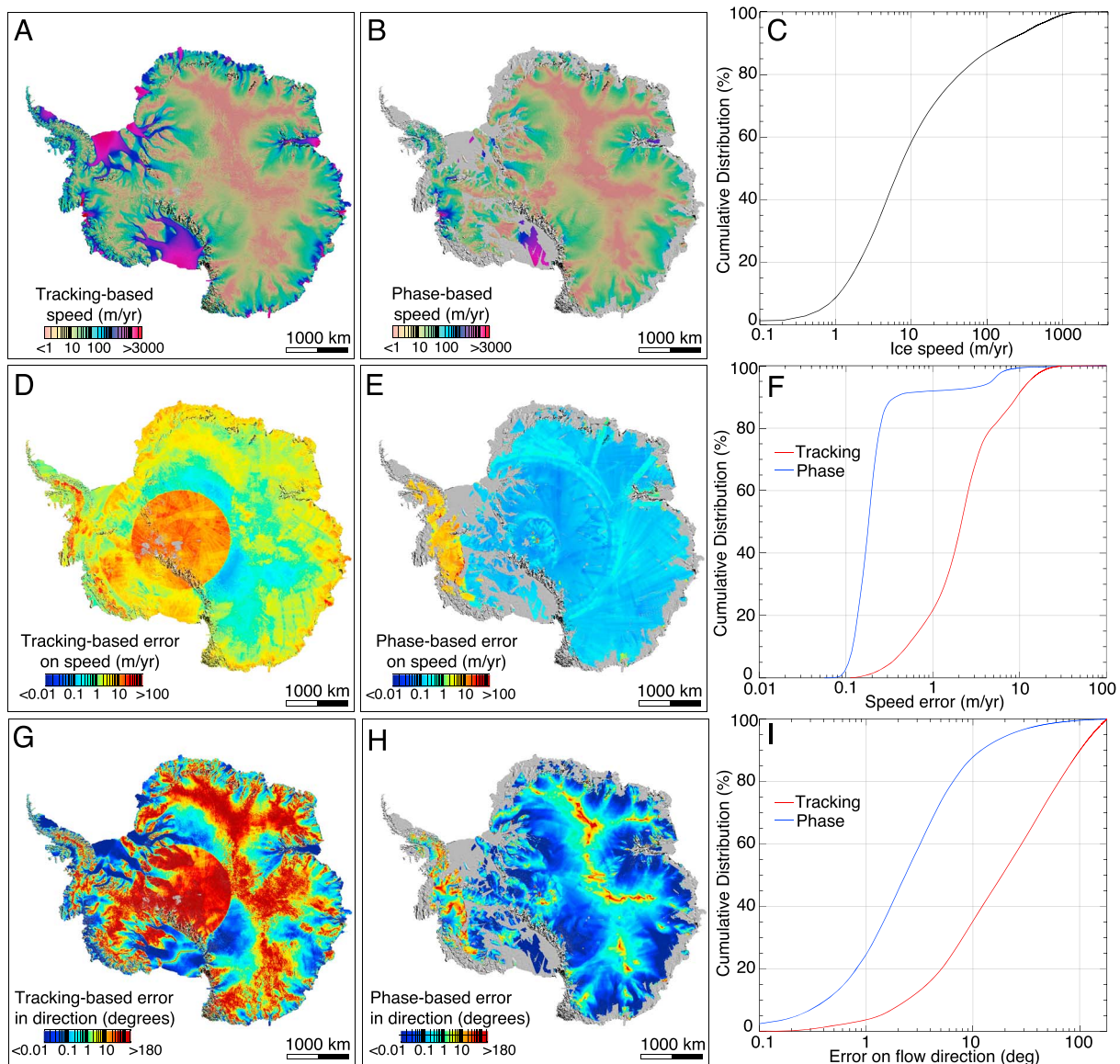


**Figure 2.** Ice flow in Antarctica from synthetic-aperture radar interferometry using (a) speckle tracking only, (b) interferometric phase only, (c) distribution of speed in meter per year across Antarctica from (a), (d) error in speckle-tracking-derived speed, (e) error in phase-only-derived speed, (f) distribution of error in speed across Antarctica for speckle tracking (red) and phase (blue) over commonly surveyed areas, (g) error in flow direction in degrees for speckle tracking, (h) for phase only, and (i) distribution of errors in flow direction over commonly surveyed areas.

SAR platforms has made it possible to obtain phase data at different look angles, over a larger share of the continent, for the first time. This mapping exercise remains limited to areas of slow flow, where the interferometric phase can be unwrapped in each pixel element. In areas of fast motion where the interferometric phase wraps too quickly within one pixel element, due to rapid rates of deformation, we can only use speckle tracking techniques.

Here, we present a phase map of Antarctic ice flow that combines data acquired by six different sensors from multiple agencies over the course of 25 years. We describe the methodology employed to process the data and assemble them into an Antarctic-wide mosaic, discuss our evaluation of the precision of the results, how we combine the phase results with speckle tracking results to form a comprehensive view of ice motion across Antarctica, and conclude on the importance of the improvement in velocity mapping for various applications, including ice sheet numerical modeling.



## 2. Materials and Methods

A SAR interferogram is formed by differencing the complex amplitude (magnitude and phase expressed as a complex number) of radar data acquired a few days apart along the same relative orbit of the spacecraft. First, the two images are coregistered so each pixel covers the same area on the ground. In the case of a moving surface like ice/snow, we correct not only for the slight horizontal offset in  $x$  and  $y$  of the two images along and across the satellite pass but also for the horizontal displacement of ice in between the passes; otherwise, the SAR signal coherence is lost when ice displacements exceed one resolution cell. This step is done by first calculating the motion field using a speckle tracking technique in two dimensions (Michel & Rignot, 1999; Mouginot et al., 2012) and displaces the pixels of the slave image accordingly to restore phase coherence of the image pair. The resulting interferogram contains signals associated with ice motion, surface topography, and image noise, which includes ionospheric noise, residual error in interferometric baseline, and perturbations associated with water vapor (Joughin, 2002). In Antarctica, the latter is generally not an issue, but the ionospheric noise is significant at the L-band frequency and even at the C-band frequency at times of high solar activity. In order to retrieve the ice flow vector, it is necessary to correct the phase data for these noise sources.

The phase shift introduced by surface topography is removed by subtracting the synthetic phase signal generated using a digital elevation model (DEM) of the surface. Here, we use the TanDEM-X DEM of Antarctica at 30-m spacing, with a vertical accuracy of 1 m (Wessel et al., 2018). The interferometric baselines are generated from the satellite precision orbits directly. In the latest generation SAR satellites, orbit information is good enough that we can remove the topographic signal with precision. With older generation SARs, for example, ERS-1/2, we first have to optimize the differential baseline before removing residual topographic fringes.

When a radar signal propagates through the ionosphere, the microwave signal experiences a phase shift and a Faraday rotation of the polarization (Meyer et al., 2006). Variations of the ionospheric delay within the synthetic aperture introduce a varying phase shift in the phase history, which is dispersive (Gray et al., 2000; Meyer, 2010). At low radar frequencies, such as L-band (1.2 GHz), the ionosphere phase shift is an important source of disturbance, which needs to be corrected. Following Liao et al. (2018), we employ a split-spectrum technique to reduce ionospheric phase shift and apply it to all L-Band ALOS/PALSAR data (Figure S1 in the supporting information). The ionospheric phase delays are considered negligible for radars operating at the C-Band frequency (e.g., ERS-1/2, Envisat ASAR, and RADARSAT-1/2).

After removing the interferometric baseline using the satellite orbits and correcting the data for ionospheric noise, the interferometric phases are unwrapped using Goldstein et al.'s (1988) algorithm. Phase unwrapping is limited by the coherence of the phase signal and phase aliasing. Obvious unwrapping errors (phase jumps) are manually masked on each individual track. The unwrapped phases are referenced and calibrated for residual baseline errors against the most recent tracking-based Antarctic composite velocity map (Mouginot et al., 2017) and converted into absolute surface displacements in ground range geometry. The residual baselines are modeled as two-dimensioned quadratic polynomial functions. Large-scale bias in the earlier mapping may propagate into the phase calibration solution but our assessment against Global Positioning System measurements indicates an absolute accuracy of about 1 m/year (Figure S7).

To combine the phase data in a geographic reference framework, we implement a cube database to access surface displacement from unwrapped phases. The database is constructed with netCDF cubes, where each cube is  $250 \times 250$  pixels ( $450 \text{ m} \times 450 \text{ m}$  per pixel) or  $12,600 \text{ km}^2$  in size, covering the entire continent. This staging procedure minimizes disk space encumbrance, especially for long tracks across the continent, and enables a natural merging of data from different platforms and different time periods onto a common grid. Unwrapped phases are staged as multiple layers, with their own heading, incidence angle, date of acquisition, and precision levels. Dividing Antarctica in cubes makes it possible to process data in parallel, hence improving computational efficiency of the mapping process.

To form a three-dimensional ice flow map from the cubes, we used the surface-parallel flow assumption (Joughin et al., 1998). For each cube, ascending and descending passes with a difference in track direction greater than  $25^\circ$  are combined to form the horizontal components ( $v_x$ ,  $v_y$ ) of the ice-flow. Surface slopes needed for estimating the vertical component ( $v_z$ ) of the flow are generated using the high-resolution

TanDEM-X DEM smoothed with an averaging filter of 5 to 10 ice thickness. As more than one combination of ascending and descending passes is possible, the horizontal velocity components are determined as the weighted mean of all possible combinations available at each output grid point. The weights are inversely proportional to the estimated error of each measurement. Additional weighting is applied at the edges of the unwrapped phase, as a “feathering” technique, to minimize discontinuities between adjacent phases.

Similar to (Joughin et al., 1998), we assume a uniform value of  $\pm\pi$  radians ( $\pm\frac{1}{2}$  cycle) for the phase error, which is conservative. We track the error in the input data and propagate it through the mosaicking and stacking processes to produce an error map of the two horizontal components. Because of differences in radar frequency, repeat cycle, and amount of source data at each point, the error maps exhibit some spatial variability (Figure 2e). In addition to the error, we compute the standard deviation in  $v_x$  and  $v_y$  from the multiple combination of ascending and descending passes (Figure S2).

In the last step, we merge the phase-derived velocity with the earlier mosaic of ice velocity derived from speckle and feature tracking (Mouginot et al., 2017). Where available, the phase data take priority. At the transition boundary, we apply a feathering technique to minimize the discontinuity in velocity and in spatial derivative in both horizontal directions, but preserving the phase data (Figure S3).

We rely on the entire SAR archive since 1992 with six sensors from multiple space agencies (Figure 1 and Table S1). The data are the Canadian Space Agency with RADARSAT-1 and RADARSAT-2, the European Space Agency (ESA) with the Earth Remote Sensing Satellites 1-2 (ERS-1/2) and the Envisat ASAR, and the Japan Aerospace Exploration Agency (JAXA) with ALOS PALSAR-1 and a few scenes from ALOS2 PALSAR. We do not include data from the European Copernicus Sentinel-1a/b SARs because the TopSAR acquisition mode of the Sentinel-1a/b data produces residual phase jumps at burst boundaries that make it impractical for precision phase-mapping, even with data stacking and additional corrections (Scheuchl et al., 2016). Each sensor has its own advantage and inconvenience: Envisat ASAR and RADARSAT-2 are the only sensors providing descending passes over East Antarctica. ALOS PALSAR-1 provides ascending passes with a high temporal coherence along the periphery. RADARSAT-2 provides the most complete dataset with coverage of the southernmost regions including ascending and descending passes in left looking mode and right looking coverage with ascending and descending passes similar to Envisat ASAR. ERS-1/2 provides high coherence images (1-day repeat) over rapidly changing sectors of West Antarctica. Phase-derived velocity is mostly for years between 2007 and 2018, while regions covered by speckle-tracking-derived velocity (along the coasts) are mostly representative of years 2013-2017. SAR and interferogram processing, unwrapping, and geocoding were done using GAMMA remote sensing processor.

### 3. Results

The unwrapped phase uses C-Band sensors ( $\lambda \sim 5.5$  cm) with 1,461 tracks from RADARSAT-1 and RADARSAT-2, 76 from ERS-1/2, 319 from Envisat ASAR, and L-Band sensors ( $\lambda \sim 23.6$  cm): 556 from ALOS/PALSAR and 3 from ALOS2/PALSAR2 (Figure 1a). The combination of phase and tracking mosaic covers 99.8% of Antarctica (Figure 1b) with a significantly improved description of ice flow from the ice divides in the deep interior to the periphery. The phase mosaic itself does not cover all of Antarctica (Figure 2b) for two reasons: (1) the interferometric phase is aliased in areas of fast flow due to the long temporal baseline of the data (except the ASE) and (2) some sectors do not have sufficient multi-track coverage to provide reliable estimates of the vector ice motion. Overall, the phase-based map covers 71% of Antarctica, or 9.9 million square kilometer, while tracking-based map covers 99.6%, or 13.8 million square kilometer (Mouginot et al., 2017). The improvement in precision is especially significant along ice divides when examining the error in flow direction.

The ionospheric correction improves the L-band phase data considerably. A comparison of phase noise before and after ionospheric corrections indicates that the phase noise is reduced by 90% in Antarctica, that is, essentially dropping from 1 m/year to 10 cm/year (Liao et al., 2018; Figure S1). Phase mapping would be impractical at L-band for speeds below 10 m/year if ionosphere noise is not compensated (Figure S1).

The noise level achievable with a single optical Landsat-8 pair ranges from 17 m/year with a 16-day cycle up to 1 m/year for exceptionally long temporal baselines of 368 days (Mouginot et al., 2017). Similar noise level

using tracking with SAR pairs is found, that is, 17 m/year with 6-day cycle to 5 m/year for 24-day cycle using Sentinel-1. We evaluate from the standard deviation between multiple phase combination that the precision of ice motion mapping from a single combination of ascending and descending interferometric phases is typically 0.1–2 m/year (Figure S2 and Table S1), therefore unmatched with any tracking techniques.

The distribution of error in flow speed (Figure 2f) after data stacking for areas mapped by both phase and tracking methods indicates that speckle/feature tracking (Figure 2d) achieves a precision of about 2–5 m/year versus 15–30 cm/year with the phase data (Figure 2e), that is, a difference of a factor 10 using 10 to 100 times less data (Figures S3–S5). Residual errors exist in areas with poor coverage or low temporal coherence, including South Pole and Central East Antarctica. Over 80% of the area mapped with phase data, the noise in ice speed is less than 30 cm/year. For comparison, less than 5% of the area mapped with speckle/feature tracking method reached that level of precision.

The higher precision in ice velocity implies a far better description of the flow direction. Over the common areas with phase and speckle tracking, the error in flow direction with phase data is less than 1° over 25% of Antarctica and less than 2° over 50% of Antarctica. With tracking methods, the error is less than 1° over only 5% of Antarctica and 13% for 2°. When we mix the two products, the error in flow direction is less than 10° over 80% of Antarctica versus 45% with tracking methods only.

The error in speed and flow direction with the phase data is higher than average over the Peninsula and ASE where we use 1-day repeat ERS-1/2 data. Conversely, we find a significant improvement in flow mapping across the Transantarctic mountains, and more broadly speaking within a circle about 1,000 km in radius around South Pole where flow directions from speckle tracking were not reliable in the past due to the low flow speed. Major improvements are also found in flow direction in vast sectors of East Antarctica, typically within  $\pm 500$  km of ice divides, where flow speed is slow and not well tracked with speckle and feature tracking.

#### 4. Discussion

In Figure 1, we display the flow speed on a logarithmic scale overlaid on the flow direction from line convolution integral techniques to visualize the vector field of ice displacement. We also show drainage boundaries of major sectors of Antarctica derived from a combination of surface slope in the interior and flow vectors along the coast from the speckle-tracking based velocity of Antarctica (Rignot et al., 2019). Surface slope is calculated using a TanDEM-X DEM of Antarctica (Wessel et al., 2018) smoothed at 10 ice thickness (Cuffey & Paterson, 2010; Gudmundsson, 2003). Along the coastline, we use flow lines emanating from the end points of ice shelves until errors in surface slope are lower than the errors in flow direction. In the new product, over the vast majority of the ice divides, flow lines align well with the direction of maximum surface slope. We note a couple of exceptions. One is the divide between Rutford Ice Stream and Pine Island Glacier, West Antarctica, where we may have overestimated the drainage area of Rutford Ice Stream in prior derivations, presumably because the position of the divide is sensitive to small errors in surface slope in that sector. In the interior basin of Academy and Support Force ice streams, East Antarctica, near South Pole, surface slope and flow direction do not exactly line up. Farther north, along the Transantarctic mountain, where ice speed is low ( $< 1$  m/year), the new flow direction is much better aligned with surface slope than in prior mappings.

The new composite map provides better information about strain rates in interior Antarctica (Figure S6). The noise level in shear strain rate calculated over 900-m grid spacing (2 pixels) drops from about  $3 \times 10^{-4}$  to less than  $1 \times 10^{-5}$  year<sup>-1</sup> over a large part of the continent. This noise level makes it possible to examine strain rates in the proximity of ice core sites in order to constrain the age of ice (Liefvering et al., 2018; Parrenin et al., 2017), but further examination of the data will be necessary to determine at a local level if the data accuracy is sufficient. We provide an error map for the velocity product. At the current level of precision, comparison with velocity and strain rate data collected near drilling sites (Richter et al., 2013; Yang et al., 2014) should be more useful (ice velocity from few cm/year to 2 m/year) compared to earlier products limited to a precision of few meters per year.

Examination of strain rates over other regions away from the ice divides in principle provides information about the rate of ice thinning or thickening if surface mass balance is known and vice versa (Reeh et al.,

1999, 2002). Alternatively, the comparison of actual velocities with balance velocities has been instrumental in evaluating new versions of surface mass balance products from regional atmospheric climate models (Agosta et al., 2019; van Wessem et al., 2018). Balance velocities require information on both surface mass balance and thickness. A comparison of Regional Atmospheric Climate Model (RACMO) Version 2.3p1 and Version 2.1, for instance, indicated major improvements with Version 2.3p1 (van Wessem et al., 2014). As new versions of RACMO, Model Atmospherique Regional (MAR) and others become available, a comparison of the revised balance velocities with the new phase map will be instrumental to evaluate the models over the Antarctic plateau in a quantitative fashion, at the regional level, to guide model evaluation and diagnosis. This work goes beyond the scope of the present study as it involves an error analysis of both products but will be pursued in the future.

Another important application of the phase map will be to extend the domain of ice thickness mapping using mass conservation (Morlighem et al., 2011, 2014, 2017), thereby extending it from narrow but important sectors of fast moving ice around the periphery to much larger areas in the interior regions. The error in flow direction is critical for extending the mass conservation technique in the interior, more than the error in speed. The error in flow direction, which is an output product, is proportional to the error in ice speed divided by the ice speed (Mouginot et al., 2017). Assuming a nominal error of 20 cm/year for the ice velocity phase-based map, we have an error of  $2.5^\circ$  or 0.05 radian for ice flowing at  $>2$  m/year (about 20% of Antarctica). With the nominal error of 2-5 m/year of the tracking-based map, the flow direction in these areas is undetermined ( $180^\circ$ ). In other words, we find that the error in flow direction is less than  $5^\circ$  over 70 % of Antarctica using the new phase map versus 30% in prior maps (Figure S4). The new map has therefore considerable potential to extend mass conservation over a much larger share of Antarctica. In the interior regions, the assumption that surface speed is identical to the depth-averaged speed will have to be reconsidered carefully, which could be done via data assimilation in an ice flow model.

In the proximity of ice divides, where ice speed drops to less than 50 cm/year, our velocity product does not account for the effect of surface mass balance; that is, the flow vector is not parallel to the ice surface but influenced by surface mass balance values. As mentioned earlier, this is an issue over less than 5% of Antarctica. It is difficult to project how much lower the data noise could be with data stacking. When ice speed drops below about 10 cm/year, we will have to include not only surface mass balance processes but also plate motion at the several cm per year level (Bouin & Vigny, 2000; Jiang et al., 2009). The mapping exercise therefore becomes more complex.

With the launch of the National Aeronautics and Space Administration ISRO NISAR mission (Rosen et al., 2016) in late 2021, with an L-band radar operating on a 12-day repeat cycle, in left (south) looking mode, we expect a performance level comparable to 46-day ALOS PALSAR when accumulating data over 3 to 4 cycles, which will be repeated 8 to 10 times a year with both ascending and descending tracks. In terms of number of phase cycles (aliasing), the 12-day repeat at L-Band would be equivalent to 2.6-day repeat at C-Band; therefore, NISAR will theoretically allow to unwrap phase data farther into fast moving areas, similar to the 1-day ERS-1/2 coverage used for West Antarctica (Figure 2b). It will therefore be potentially possible to obtain a similar quality phase map, with a spatial coverage greater than 71% and or even 85%, within one year of operation as opposed to 25 years herein.

## 5. Conclusions

In this study, we combined interferometric phase data from a series of SAR satellites acquired over 25 years, with a concentration of data ramping up in the last 10 years. This ensemble of data enables a near complete phase mapping of the interior regions of Antarctica at an unprecedented level of precision. The results offer precision mapping, at a level of 20 cm/year in speed and  $5^\circ$  in flow direction, over 70% of Antarctica. This digital product is 10 times superior to that generated from feature and speckle tracking techniques. The results will be instrumental to revise ice drainage, analyze strain rates, extend the mapping of ice thickness from mass conservation technique to much broader areas, and other applications requiring precision ice flow mapping. In turn, the phase map of Antarctica will provide a more complete and comprehensive view on ice velocity to ice sheet numerical models in the vast interior of the continent.



## Acknowledgments

The authors thank K. Cuffey and A. Gardner for valuable feedback on an early draft of this manuscript. This work was performed at the University of California Irvine and at Caltech's Jet Propulsion Laboratory under contracts with the National Aeronautics and Space Administration's Make Earth System Data Records for Use in Research Environments (MEaSUREs) program and with the Cryosphere Science Program. J. M. acknowledges funding from the French Centre National d'Etudes Spatiales (CNES). We thank data grants from the Canadian, European, and Japanese Space Agencies with the help of Henri Laur (ESA), Yves Crevier (CSA), and Masanobu Shimada (JAXA), under the umbrella of the Polar Space Task Group (PSTG) for data acquisition and distribution worldwide. The authors further thank the German Space Agency (DLR) for providing the TANDEM-X DEM. Ice motion products from this study are available as MEaSUREs products at the National Snow and Ice Data Center (NSIDC), Boulder, CO, DOI: <https://doi.org/10.5067/PZ3NJ5RHRH10>.

## References

- Agosta, C., Amory, C., Kittel, C., Orsi, A., Favier, V., Gallée, H., et al. (2019). Estimation of the Antarctic surface mass balance using the regional climate model MAR (1979–2015) and identification of dominant processes. *The Cryosphere*, 13(1), 281–296. <https://doi.org/10.5194/tc-13-281-2019>
- Bouin, M.-N., & Vigny, C. (2000). New constraints on Antarctic plate motion and deformation from GPS data. *Journal of Geophysical Research*, 105(B12), 28,279–28,293. <https://doi.org/10.1029/2000JB900285>
- Cuffey, K. M., & Paterson, W. S. B. (2010). *The Physics of Glaciers*. Amsterdam: Academic Press.
- Goldstein, R. M., Zebker, H. A., & Werner, C. L. (1988). Satellite radar interferometry: Two-dimensional phase unwrapping. *Radio Science*, 23(4), 713–720. <https://doi.org/10.1029/RS023i004p00713>
- Goldstein, R. M., Engelhardt, H., Kamb, B., & Frolich, R. M. (1993). Satellite radar interferometry for monitoring ice sheet motion: Application to an Antarctic ice stream. *Science*, 262(5139), 1525–1530. <https://doi.org/10.1126/science.262.5139.1525>
- Gray, A. L., Mattar, K. E., & Sofko, G. (2000). Influence of ionospheric electron density fluctuations on satellite radar interferometry. *Geophysical Research Letters*, 27(10), 1451–1454. <https://doi.org/10.1029/2000GL000016>
- Gray, L. (2011). Using multiple RADARSAT InSAR pairs to estimate a full three-dimensional solution for glacial ice movement. *Geophysical Research Letters*, 38, L05502. <https://doi.org/10.1029/2010GL046484>
- Gudmundsson, G. H. (2003). Transmission of basal variability to a glacier surface. *Journal of Geophysical Research*, 108(B5), 2253. <https://doi.org/10.1029/2002JB002107>
- Jiang, W.-P., Dong-Chen, E., Zhan, B.-W., & Liu, Y.-W. (2009). New Model of Antarctic Plate Motion and Its Analysis. *Chinese Journal of Geophysics*, 52(1), 23–32. <https://doi.org/10.1002/cjg2.1323>
- Joughin, I. (2002). Ice-sheet velocity mapping: a combined interferometric and speckle-tracking approach. *Annals of Glaciology*, 34, 195–201. <https://doi.org/10.3189/172756402781817978>
- Joughin, I., Smith, B. E., & Howat, I. (2018). Greenland Ice Mapping Project: Ice flow velocity variation at sub-monthly to decadal time-scales. *The Cryosphere*, 12(7), 2211–2227. <https://doi.org/10.5194/tc-12-2211-2018>
- Joughin, I., Smith, B. E., Howat, I. M., Scambos, T., & Moon, T. (2010). Greenland flow variability from ice-sheet-wide velocity mapping. *Journal of Glaciology*, 56(197), 415–430. <https://doi.org/10.3189/002214310792447734>
- Joughin, I. R., Kwok, R., & Fahnestock, M. A. (1998). Interferometric estimation of three-dimensional ice-flow using ascending and descending passes. *IEEE Transactions on Geoscience and Remote Sensing*, 36(1), 25–37. <https://doi.org/10.1109/36.655315>
- Liao, H., Meyer, F. J., Scheuchl, B., Mouginot, J., Joughin, I., & Rignot, E. (2018). Ionospheric correction of InSAR data for accurate ice velocity measurement at polar regions. *Remote Sensing of Environment*, 209, 166–180. <https://doi.org/10.1016/j.rse.2018.02.048>
- Lieffering, B. V., Pattyn, F., Cavitte, M. G. P., Karlsson, N. B., Young, D. A., Sutter, J., & Eisen, O. (2018). Promising Oldest Ice sites in East Antarctica based on thermodynamical modelling. *The Cryosphere*, 12(8), 2773–2787. <https://doi.org/10.5194/tc-12-2773-2018>
- Massonnet, D., Rossi, M., Carmona, C., Adragna, F., Peltzer, G., Feigl, K., & Rabaute, T. (1993). The displacement field of the Landers earthquake mapped by radar interferometry. *Nature*, 364(6433), 138–142. <https://doi.org/10.1038/364138a0>
- Meyer, F. (2010). A review of ionospheric effects in low-frequency SAR—Signals, correction methods, and performance requirements. In *2010 IEEE International Geoscience and Remote Sensing Symposium* (pp. 29–32). <https://doi.org/10.1109/IGARSS.2010.5654258>
- Meyer, F., Bamler, R., Jakowski, N., & Fritz, T. (2006). The potential of low-frequency SAR systems for mapping ionospheric TEC distributions. *IEEE Geoscience and Remote Sensing Letters*, 3(4), 560–564. <https://doi.org/10.1109/LGRS.2006.882148>
- Michel, R., & Rignot, E. (1999). Flow of Glaciér Moreno, Argentina, from repeat-pass Shuttle Imaging Radar images: comparison of the phase correlation method with radar interferometry. *Journal of Glaciology*, 45(149), 93–100. <https://doi.org/10.1017/S0022143000003075>
- Morlighem, M., Rignot, E., Mouginot, J., Seroussi, H., & Larour, E. (2014). High-resolution ice-thickness mapping in South Greenland. *Annals of Glaciology*, 55(67), 64–70. <https://doi.org/10.3189/2014AoG67A088>
- Morlighem, M., Rignot, E., Seroussi, H., Larour, E., Dhia, H. B., & Aubry, D. (2011). A mass conservation approach for mapping glacier ice thickness. *Geophysical Research Letters*, 38, L19503. <https://doi.org/10.1029/2011GL048659>
- Morlighem, M., Williams, C. N., Rignot, E., An, L., Arndt, J. E., Bamber, J. L., et al. (2017). BedMachine v3: Complete bed topography and ocean bathymetry mapping of Greenland from multibeam echo sounding combined with mass conservation. *Geophysical Research Letters*, 44, 11,051–11,061. <https://doi.org/10.1002/2017GL074954>
- Mouginot, J., Rignot, E., Björk, A. A., van den Broeke, M., Millan, R., Morlighem, M., et al. (2019). Forty-six years of Greenland Ice Sheet mass balance from 1972 to 2018. *Proceedings of the National Academy of Sciences*, 116, 9239–9244. <https://doi.org/10.1073/pnas.1904242116>
- Mouginot, J., Rignot, E., Scheuchl, B., & Millan, R. (2017). Comprehensive annual ice sheet velocity mapping using Landsat-8, Sentinel-1, and RADARSAT-2 data. *Remote Sensing*, 9(4), 364. <https://doi.org/10.3390/rs9040364>
- Mouginot, J., Scheuchl, B., & Rignot, E. (2012). Mapping of ice motion in Antarctica using synthetic-aperture radar data. *Remote Sensing*, 4(9), 2753–2767. <https://doi.org/10.3390/rs4092753>
- Nagler, T., Rott, H., Hetzenecker, M., Wuite, J., & Potin, P. (2015). The Sentinel-1 mission: New opportunities for ice sheet observations. *Remote Sensing*, 7(7), 9371–9389. <https://doi.org/10.3390/rs70709371>
- Parrenin, F., Cavitte, M. G. P., Blankenship, D. D., Chappellaz, J., Fischer, H., Gagliardini, O., et al. (2017). Is there 1.5-million-year-old ice near Dome C, Antarctica? *The Cryosphere*, 11(6), 2427–2437. <https://doi.org/10.5194/tc-11-2427-2017>
- Reeh, N., Madsen, S. N., & Mohr, J. J. (1999). Combining SAR interferometry and the equation of continuity to estimate the three-dimensional glacier surface-velocity vector. *Journal of Glaciology*, 45(151), 533–538. <https://doi.org/10.3189/S0022143000001398>
- Reeh, N., Mohr, J. J., Krabill, W. B., Thomas, R., Oerter, H., Gundestrup, N., & Bøggild, C. E. (2002). Glacier specific ablation rate derived by remote sensing measurements. *Geophysical Research Letters*, 29(16), 10–1. <https://doi.org/10.1029/2002GL015307>
- Richter, A., Fedorov, D. V., Fritsche, M., Popov, S. V., Lipenkov, V. Y., Ekaykin, A. A., et al. (2013). Ice flow velocities over Vostok Subglacial Lake, East Antarctica, determined by 10 years of GNSS observations. *Journal of Glaciology*, 59(214), 315–326. <https://doi.org/10.3189/2013JG12J056>
- Rignot, E., & Mouginot, J. (2012). Ice flow in Greenland for the International Polar Year 2008–2009. *Geophysical Research Letters*, 39, L11501. <https://doi.org/10.1029/2012GL051634>
- Rignot, E., Mouginot, J., & Scheuchl, B. (2011). Ice flow of the Antarctic Ice Sheet. *Science*, 333(6048), 1427–1430. <https://doi.org/10.1126/science.1208336>
- Rignot, E., Mouginot, J., Scheuchl, B., van den Broeke, M., van Wessem, M. J., & Morlighem, M. (2019). Four decades of Antarctic Ice Sheet mass balance from 1979–2017. *Proceedings of the National Academy of Sciences*, 116(4), 1095–1103. <https://doi.org/10.1073/pnas.1812883116>



- Rignot, E., Thomas, R. H., Kanagaratnam, P., Casassa, G., Frederick, E., Gogineni, S., et al. (2004). Improved estimation of the mass balance of glaciers draining into the Amundsen Sea sector of West Antarctica from the CECS/NASA 2002 campaign. *Annals of Glaciology*, 39, 231–237. <https://doi.org/10.3189/172756404781813916>
- Rosen, P. A., Hensley, S., Shaffer, S., Edelstein, W. N., Kim, Y., Kumar, R., et al. (2016). An update on the NASA-ISRO dual-frequency DBF SAR (NISAR) mission. In *2016 IEEE International Geoscience and Remote Sensing Symposium (IGARSS)* (pp. 2106–2108). <https://doi.org/10.1109/IGARSS.2016.7729543>
- Scheuchl, B., Mougnot, J., Rignot, E., Morlighem, M., & Khazendar, A. (2016). Grounding line retreat of Pope, Smith, and Kohler Glaciers, West Antarctica, measured with Sentinel-1a radar interferometry data. *Geophysical Research Letters*, 43, 8572–8579. <https://doi.org/10.1002/2016GL069287>
- van Wessem, J. M., Reijmer, C. H., Morlighem, M., Mougnot, J., Rignot, E., Medley, B., et al. (2014). Improved representation of East Antarctic surface mass balance in a regional atmospheric climate model. *Journal of Glaciology*, 60(222), 761–770. <https://doi.org/10.3189/2014JoG14J051>
- van Wessem, J. M., van de Berg, W. J., Noël, B. P. Y., van Meijgaard, E., Amory, C., Birnbaum, G., et al. (2018). Modelling the climate and surface mass balance of polar ice sheets using RACMO2 – Part 2: Antarctica (1979–2016). *The Cryosphere*, 12(4), 1479–1498. <https://doi.org/10.5194/tc-12-1479-2018>
- Wessel, B., Huber, M., Wohlfart, C., Marschall, U., Kosmann, D., & Roth, A. (2018). Accuracy assessment of the global TanDEM-X digital elevation model with GPS data. *ISPRS Journal of Photogrammetry and Remote Sensing*, 139, 171–182. <https://doi.org/10.1016/j.isprsjprs.2018.02.017>
- Yang, Y., Sun, B., Wang, Z., Ding, M., Hwang, C., Ai, S., et al. (2014). GPS-derived velocity and strain fields around Dome Argus, Antarctica. *Journal of Glaciology*, 60(222), 735–742. <https://doi.org/10.3189/2014JoG14J078>